



Ore-blending optimization for Canadian iron concentrate during iron ore sintering based on high-temperature characteristics of fines and nuclei

Sheng-li Wu¹ · Xiao-bo Zhai¹ · Li-xin Su¹ · Xu-dong Ma¹

Received: 21 May 2019 / Revised: 23 July 2019 / Accepted: 28 July 2019 / Published online: 25 September 2019
© China Iron and Steel Research Institute Group 2019

Abstract

Canadian iron concentrate (CIC) can elevate the ferrous grade and lower the contents of gangue components and harmful elements in the sinter. To understand high-temperature characteristics of CIC and typical iron ore, the formation of the melt was calculated mainly through FactSage 7.2, and melt fluidity (MF) test for iron ore fines and penetration characteristic test of CIC melt into iron ore nuclei were carried out via micro-sintering method. The results show that hematite, calcium ferrites, dicalcium silicate, and magnetite take part in the formation of the melt in N₂. The formation temperature of the liquid for CIC is higher than that for hematite/limonite ore. The MF of CIC is lower than that of hematite/limonite ore fines. The MF of hematite/limonite ore fines is dominated by the liquid amount and melt viscosity. The penetration depth (PD) of CIC melt into limonite ore nuclei is smaller than that into hematite ore nuclei. The PD is related to the reaction ability of the nuclei with the melt. Based on above results, sinter pot tests were conducted. The result shows that in the base ore blends including two hematite ores and two limonite ores, adding CIC deteriorates the sintering indexes. Increasing the proportion of high-MF and small-PD hematite ore can significantly improve the sintering indexes. 10 mass% is a suitable proportion for adding CIC in ore blends.

Keywords Canadian iron concentrate · Iron ore sintering · Melt fluidity · Penetration depth · Ore-blending optimization

1 Introduction

In recent years, with the rapid development of the iron and steel industry, high-quality iron ore resources have been gradually depleted worldwide [1]. Moreover, the ferrous grade of iron ore has decreased, whereas the contents of gangue components and harmful impurities in iron ore have increased. Under this background, mining enterprises begin to increase the production of iron concentrates to meet the demands of the market. Canadian iron concentrate (CIC) has very high ferrous grade and low contents of Al₂O₃, crystal water, and harmful elements [2]. This provides a good condition for its ore-blending with other low-grade iron ore during sintering. Based on this, more and

more steel enterprises in China start to add CIC in ore blends to improve the quality of the sinter.

Iron ore sintering is a process of agglomerating the mixture of iron ore, flux, and fuel into the sinter, which is the main iron-bearing burden for blast furnace ironmaking in China. Before sintering, quasiparticles are formed from the layering of adhering fines (– 0.5 mm) onto nuclei particles (+ 0.5 mm) in the granulation process [3]. CIC mainly acts as the adhering fines because of its extremely high proportion of fines (+ 93 mass%), which may influence the granulation effectiveness of the quasiparticles and hence the permeability of the sintering bed. However, the granulation behavior of iron concentrates has been strengthened through some effective methods, such as ore-blending optimization [4, 5], pretreatment of iron concentrates [6–8], and modification of bonding medium [9].

During heating, high-temperature melt generates within the adhering fines by forming low-melting-point materials. The melt flows among the quasiparticles and penetrates into (reacts with) iron ore nuclei to form secondary melt

✉ Xiao-bo Zhai
xiaobo_zhai@sina.com

¹ School of Metallurgical and Ecological Engineering,
University of Science and Technology Beijing,
Beijing 100083, China

[10]. High-temperature characteristics of iron ore, especially the melt fluidity (MF) of iron ore fines and penetration characteristic of the melt into iron ore nuclei, play important roles in the bonding of the quasiparticles and the strength of the sinter [10–15]. An et al. [2] and Xiao et al. [16] found that when the basicity (CaO/SiO_2) of the adhering fines is fixed, CIC has good MF. However, in real adhering fines, each particle of iron ore fines has the same chance as each other to get in touch with lime without considering the segregation of lime. Hence, fixed proportion of lime is a more suitable condition than fixed basicity [14]. The MF of CIC at fixed proportion of lime is not clear. In addition, Yang [17] utilized Chinese iron concentrates as the adhering fines to investigate the reactivity between the melt and different iron ore nuclei through measuring the volume percent of relict ore nuclei. Nevertheless, Chinese iron concentrates had higher contents of FeO and gangue components than CIC, and Yang [17] neglected the effects of iron ore nuclei on the viscosity and amount of the melt. In general, there is limited research on high-temperature characteristics of CIC and further ore-blending optimization.

In this study, focusing on CIC and four kinds of typical iron ores, MF test of iron ore fines and penetration characteristic test of CIC melt into iron ore nuclei were carried out via the micro-sintering method. Before these tests, the formation of the melt was studied mainly through the theoretical calculation of commercial software FactSage 7.2. Based on obtained high-temperature characteristics of fines and nuclei, the schemes of sinter pot test were designed and conducted to study the effect of CIC on sintering indexes and explore ore-blending optimization methods for CIC.

2 Experimental

2.1 Raw materials

Five kinds of iron ores were used in the present study. Their chemical composition (fines: -0.5 mm and nuclei: $+0.5$ mm), proportion of fines, and major iron minerals are given in Table 1. The major iron minerals were determined by X-ray diffraction (XRD) analysis. OA and OB belong to hematite ore, from Brazil. OC and OD belong to limonite ore, from Australia.

2.2 MF test

MF is defined as the flowability of the melt generated from the reaction between iron ore fines and lime during sintering. In this study, the melt may contain liquids and a small amount of solids. Generally, high MF of iron ore

fines can enlarge the bonding extent of the melt among the quasiparticles, increasing the bonding strength of the sinter [13]. -0.5 mm particles of CIC and OA–OD were crushed into -0.074 mm fines. Each kind of fines and 15 mass% CaO reagent were mixed homogeneously to simulate different adhering fines. Out of the need of blast furnace ironmaking, the CaO content, SiO_2 content, and binary basicity ($R = w(\text{CaO})/w(\text{SiO}_2)$) of the actual sinter are fixed in a period of time through adjusting the proportion of fluxes (basic and acidic). For typical blending materials, the fluxes mostly enter into the adhering fines because of their smaller particle size. Therefore, under an almost fixed mass ratio of nuclei particles to adhering fines, the CaO content of the adhering fines is considered to be unchanged, whereas the binary basicity of the adhering fines may change owing to different SiO_2 contents of iron ore fines. In the test, the CaO content of the adhering fines was determined based on the composition of the practical blending materials [10, 14, 18]. One gram of adhering fines was pressed using hydraulic press under a pressure of 15 MPa into a cylindrical tablet with a diameter of 8 mm. Subsequently, the tablet was sintered in an infrared high-speed heating furnace shown in Fig. 1. Figure 2 shows the sintering thermal profile [18]. The flow rates of air and N_2 (oxygen partial pressure $p_{\text{O}_2} = 101.325$ Pa) were 3 L min^{-1} . 11.5 min later, the specimen was removed outside the furnace and quenched by air. After cooling, the melt fluidity index of iron ore fines was measured using Eq. (1).

$$\omega = \frac{S_a - S_b}{S_b}, \quad (1)$$

where ω is the melt fluidity index of iron ore fines; S_b is the initial area of the tablet before the test, mm^2 ; and S_a is the fluid area of the melt after the test, mm^2 . S_b was calculated by the area formula, and S_a was measured through vertical projection and image processing [11].

2.3 Penetration characteristic test

In addition to the MF of iron ore fines, the penetration characteristics of CIC melt into other iron ore nuclei were investigated as the basis of ore-blending optimization for CIC. 3.5 g of $+0.5$ mm particles of OA–OD was crushed into -0.074 mm fines and then shaped under a pressure of 30 MPa into a cylindrical tablet with a diameter of 20 mm to simulate iron ore nuclei. CIC adhering fines in the MF test act as the adhering fines. One gram of the adhering fines was shaped under a pressure of 15 MPa into a cylindrical tablet with a diameter of 8 mm. The tests were carried out in the infrared high-speed heating furnace using a couple of tablets to simulate a typical quasiparticle structure, as shown in Fig. 3.

Table 1 Chemical composition, proportion of fines, and major iron minerals of iron ore (mass%)

Iron ore	Chemical composition							Proportion of fines	Major iron mineral
	TFe	FeO	SiO ₂	CaO	Al ₂ O ₃	MgO	LOI ^a		
CIC	65.19	13.96	4.35	0.62	0.19	0.62	– ^b	93.17	Hematite and magnetite
OA									
Fines	65.87	0.67	1.39	0.02	1.13	0.03	2.63	30.08	Hematite
Nuclei	65.32	0.16	1.81	0.04	1.37	0.10	2.32		
OB									
Fines	62.13	0.83	7.82	0.04	1.01	0.07	1.96	66.30	Hematite
Nuclei	62.49	0.54	7.08	0.02	1.03	0.10	1.96		
OC									
Fines	58.35	0.28	4.39	0.06	1.57	0.08	10.46	18.01	Goethite and hematite
Nuclei	58.28	0.14	4.22	0.02	1.65	0.10	10.42		
OD									
Fines	56.81	0.27	6.11	0.06	1.72	0.09	10.74	10.15	Goethite and hematite
Nuclei	57.43	0.19	5.92	0.02	1.41	0.10	10.04		

^aLOI is loss on ignition

^bFor CIC, at high temperature, with escape of small amounts of crystal water and CO₂, oxidation of Fe₃O₄ occurs

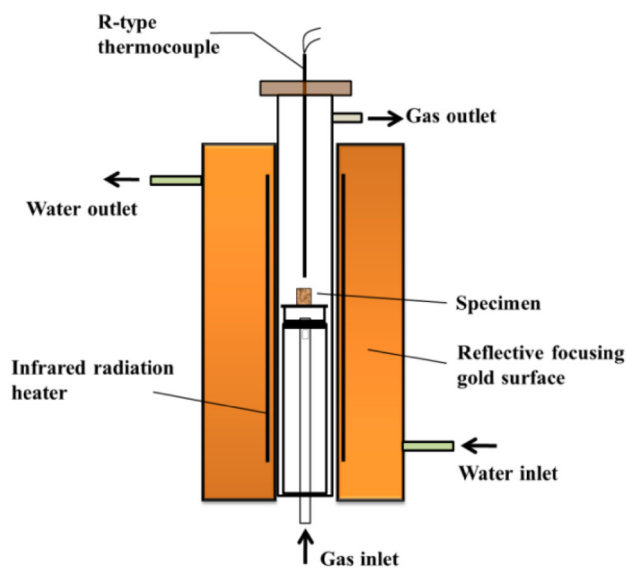


Fig. 1 Infrared high-speed heating furnace

The sintering thermal profile is the same as that in the MF test. The sintered specimens were embedded with resin and then vertically cut along with the center. The cross section of the specimens was ground and polished to obtain a smooth surface. The integrated images of the cross section were obtained using a Leica DM4 optical microscope. As shown in Fig. 3, d was used to represent the average penetration depth of CIC melt, indicating the penetration characteristic of CIC melt into iron ore nuclei. The penetration depth (PD) of CIC melt was measured from the

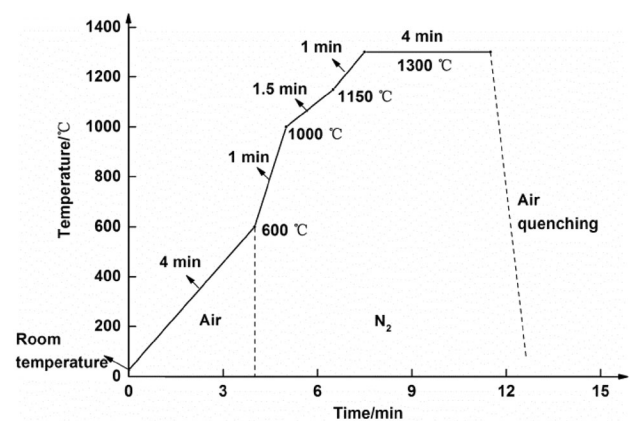


Fig. 2 Sintering thermal profile

upper surface of iron ore nuclei to the melt penetration boundary through image processing.

3 Results and discussion

3.1 Theoretical calculation of formation of melt

Before discussing the MF of iron ore fines, the formation of the melt was investigated theoretically according to the conditions of temperature and atmosphere in the MF test. According to Fig. 2, the atmosphere was transformed from air into N₂ ($p_{O_2} = 101.325$ Pa) at 600 °C owing to the combustion of coke breeze and hence the decrease in oxygen partial pressure during the actual sintering. Table 1

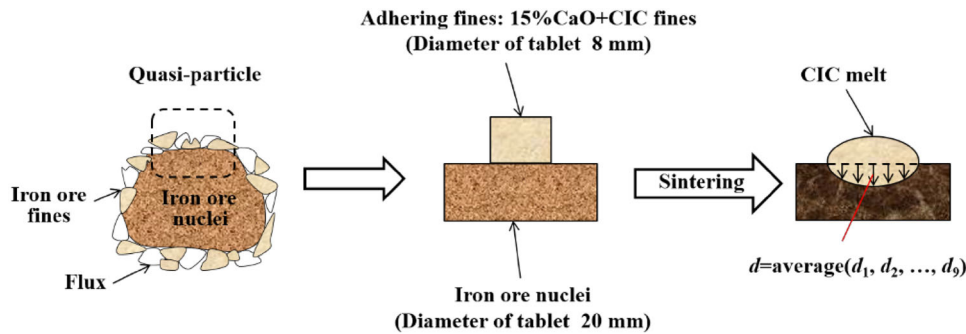
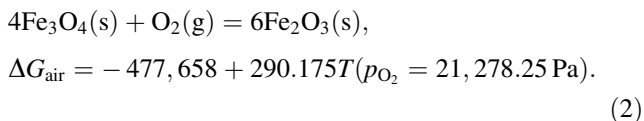


Fig. 3 Schematic of a typical quasiparticle structure and penetration characteristic of CIC melt into iron ore nuclei

shows that the major iron minerals of CIC are hematite and magnetite, and the chemical components of other iron ore contain FeO. The chemical composition of the adhering fines (including the amounts and contents of magnetite and hematite) at 600 °C in air will become the initial condition of theoretical calculation for the formation of the melt (1120–1300 °C) in N_2 ($p_{O_2} = 101.325$ Pa). Therefore, the oxidation of magnetite and the release of heat over the range from room temperature to 600 °C need to be considered.

The oxidation reaction of magnetite and Gibbs free energy change of the reaction in air ΔG_{air} is shown in Eq. (2) [19].



According to this equation, before the temperature increases to 600 °C, ΔG_{air} is less than 0, meaning that the oxidation of magnetite can occur.

In order to obtain the amounts of magnetite and hematite in CIC adhering fines at 600 °C, 1 g of CIC adhering fines was heated at a rate of roughly $144 \text{ }^\circ\text{C min}^{-1}$ (same as that in Fig. 2) from room temperature to 600 °C in air and in high-purity N_2 ($p_{O_2} = 0.101$ Pa), respectively. In high-purity N_2 , because the oxidation of magnetite is extremely weak and the decomposition of hematite is impossible (the condition of decomposition: + 945 °C) [19], the amounts of magnetite and hematite are considered as unchanged in this process. Through measuring, the masses of CIC adhering fines in the two atmospheres reduce by 0.0017 and 0.0095 g, respectively. Therefore, in the MF test of CIC adhering fines, 0.0078 g of O_2 took part in the oxidation of magnetite until 600 °C. For other iron ore adhering fines with small amounts of magnetite, all the magnetite can be easily oxidized by 0.0078 g of O_2 into hematite.

When 1 g of O_2 reacts with magnetite, the oxidation of magnetite releases 14,337.05 J heat [17]. When the

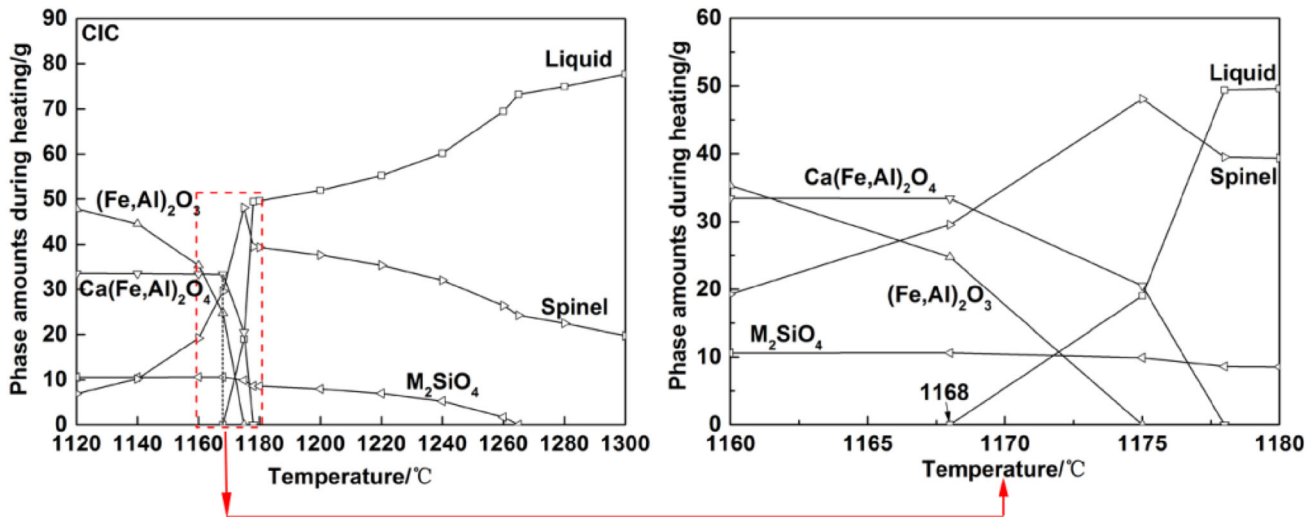
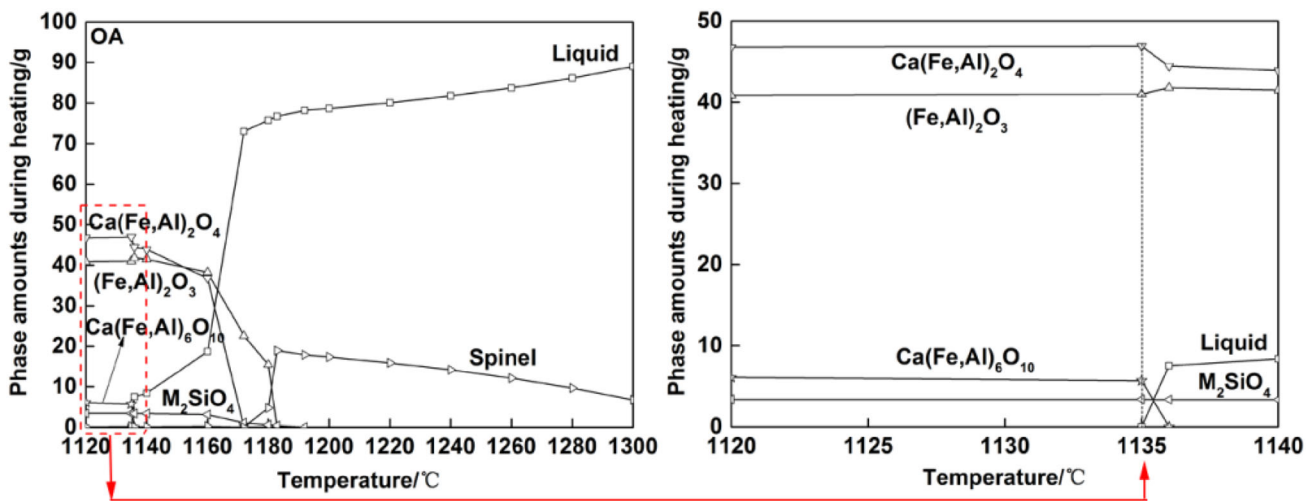
temperature reaches 600 °C, the heat from the oxidation of magnetite in 1 g of CIC adhering fines is 111.83 J. When 1 g of carbon is completely oxidized, generated heat is 32,961.26 J [17]. If coke breeze contains roughly 87 mass% carbon, the heat from the oxidation of magnetite in 1 g of CIC adhering fines is equivalent to approximately 0.004 g of coke. Thus, the heat quantity and potential to reduce coke are relatively small. The effects of the heat quantity on the temperature in the MF test and usage amount of coke breeze in sinter pot test can be neglected.

The Equilib module of FactSage 7.2 [20] was used to calculate the amount and composition of the melt over the range of 1120–1300 °C. The FToxid and FactPS were chosen as the databases of oxides and gas, respectively. In the MF test, the mass of iron ore adhering fines was 1 g. To carry out the calculation conveniently, the amount of adhering fines was expanded as 100 g (100 times). When the temperature reaches 600 °C, the magnetite in CIC adhering fines was oxidized by 0.78 g (corresponding 100 times) of oxygen. The amount and composition of the adhering fines without LOI at 600 °C are determined as given in Table 2. This can be used as the initial condition of FactSage calculation for the formation of the melt over the range of 1120–1300 °C in N_2 ($p_{O_2} = 101.325$ Pa). During sintering, LOI almost completely escapes from iron ore fines before the formation of the melt [15]. Therefore, the total amount of each adhering fines in the front of the slash in Table 2 is less than 100 g, whereas the total fraction in the back of the slash equals 100 mass%.

Figures 4–8 show the calculated phase amounts in the melts of CIC and OA–OD over the range of 1120–1300 °C, respectively. In these figures, the melt contains liquid and some solids. $(\text{Fe, Al})_2\text{O}_3$ is hematite (Fe_2O_3) containing a small amount of dissolved Al_2O_3 . The main component of spinel is magnetite (Fe_3O_4) containing some composite oxides of Fe, Al, and Mg. M_2SiO_4 is dicalcium silicate (Ca_2SiO_4) containing dissolved Fe_2SiO_4 and Mg_2SiO_4 . $\text{Ca}(\text{Fe, Al})_2\text{O}_4$ and $\text{Ca}(\text{Fe, Al})_6\text{O}_{10}$ are calcium ferrites CaFe_2O_4 and $\text{CaFe}_6\text{O}_{10}$ containing small amounts of

Table 2 Amount and composition of adhering fines without LOI at 600 °C (g/mass%)

Adhering fines	Fe ₂ O ₃	Fe ₃ O ₄	SiO ₂	CaO	Al ₂ O ₃	MgO	Total
CIC	63.01/63.94	15.61/15.85	3.70/3.75	15.53/15.76	0.16/0.16	0.53/0.53	98.53/100.00
OA	79.99/82.31	0.00/0.00	1.18/1.22	15.02/15.45	0.96/0.99	0.03/0.03	97.17/100.00
OB	75.44/76.95	0.00/0.00	6.65/6.78	15.03/15.33	0.86/0.88	0.06/0.06	98.04/100.00
OC	70.85/77.83	0.00/0.00	3.73/4.10	15.05/16.53	1.33/1.47	0.07/0.07	91.04/100.00
OD	68.98/76.00	0.00/0.00	5.19/5.72	15.05/16.58	1.46/1.61	0.08/0.08	90.77/100.00

**Fig. 4** Calculated phase amounts in CIC melt during heating**Fig. 5** Calculated phase amounts in OA melt during heating

dissolved CaAl_2O_4 and $\text{CaAl}_6\text{O}_{10}$, respectively. These solids are formed through solid-state reactions before the formation of the liquid [21] and not described in detail owing to the limited space. For different iron ores, the dissolution amount of dissolved materials in these solids at different temperatures is different.

Figure 9 shows the calculated O_2 amounts released from the melts during heating through the equilibrium calculation of FactSage. From Fig. 9, as a whole, iron oxides in the melts decompose to release oxygen. When the temperature of the melt is below 1175 °C for CIC and 1183 °C for OA–OD, the decomposition extent is drastic; however,

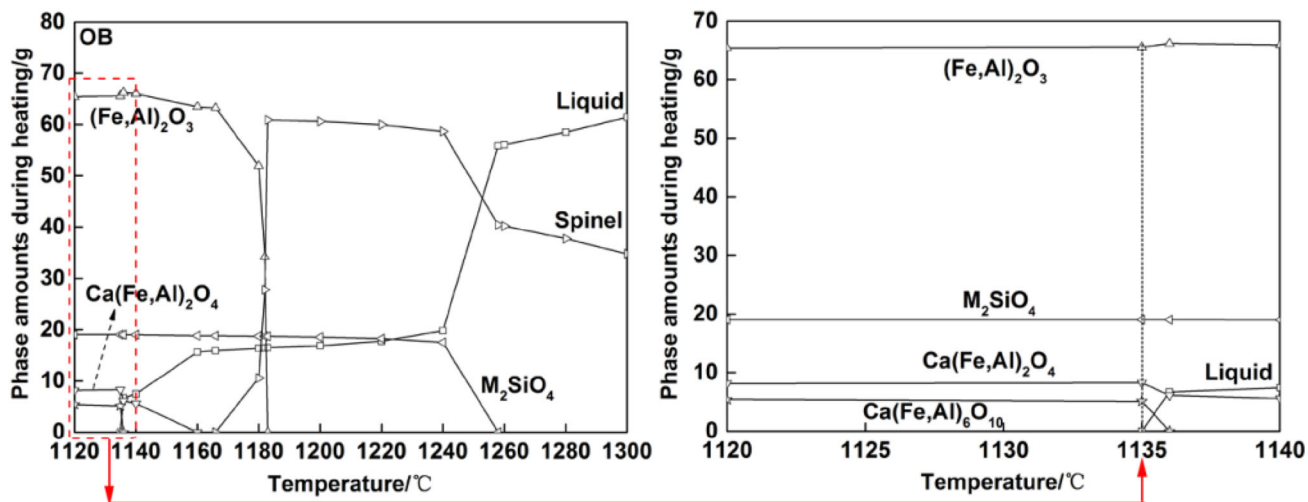


Fig. 6 Calculated phase amounts in OB melt during heating

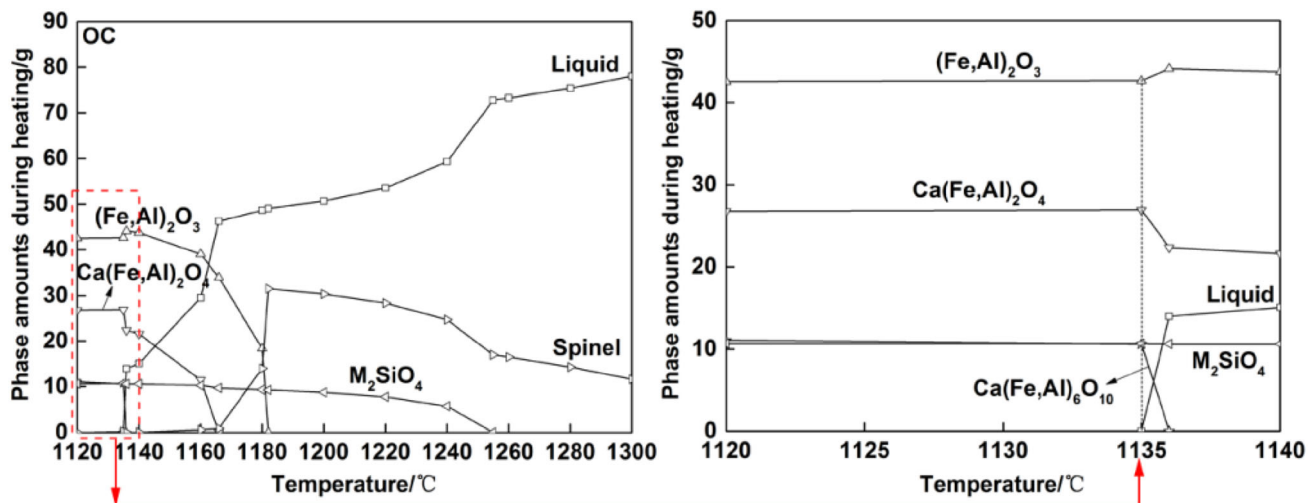


Fig. 7 Calculated phase amounts in OC melt during heating

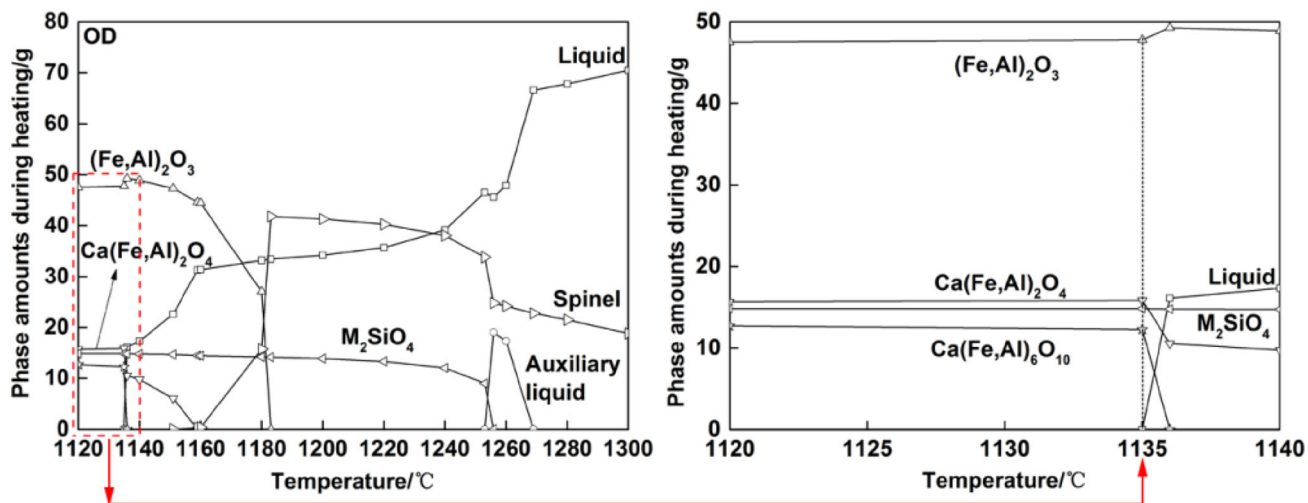


Fig. 8 Calculated phase amounts in OD melt during heating

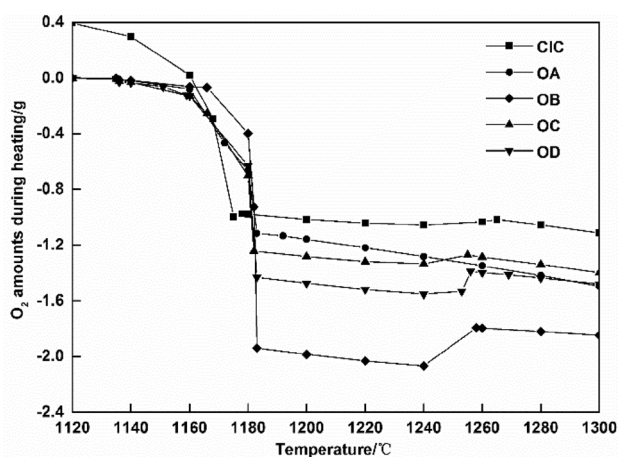


Fig. 9 Calculated O_2 amounts released from CIC and OA–OD melts during heating. Positive value indicates absorption, whereas negative value indicates release

when the temperature exceeds the corresponding values, the decomposition extent is slow. As shown in Figs. 4–8, at 1175 °C for CIC melt and 1183 °C for OA–OD melts, $(Fe, Al)_2O_3$ is consumed out mainly owing to the decomposition to spinel. As shown in Fig. 10, in N_2 ($p_{O_2} = 101.325$ Pa), the decomposition of Fe_2O_3 is easier than that of Fe_3O_4 [19]. Therefore, it is speculated that the decomposition of Fe_2O_3 becomes dominant during drastic stage, while the decomposition of Fe_3O_4 becomes dominant during slow stage.

In addition, there is a brief oxidation stage over the range of roughly 1240–1265 °C for CIC melt and 1240–1260 °C for OB–OD melts. In contrast to Figs. 4 and 6–8, the dissolution extent of M_2SiO_4 over the range is sharper than that of M_2SiO_4 over other ranges. It is inferred that Fe_2SiO_4 in M_2SiO_4 is oxidized and dissolved in the liquid. However, there is no oxidation stage for OA. A

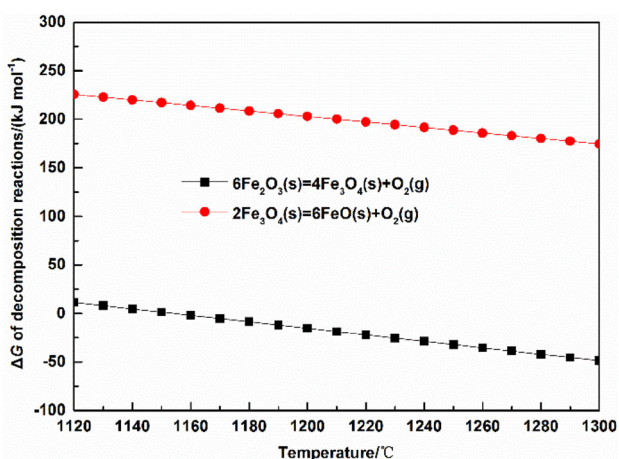


Fig. 10 ΔG of decomposition reactions of iron oxides in N_2 ($p_{O_2} = 101.325$ Pa)

possible reason for this is that OA has the lowest SiO_2 content, leading to the lowest M_2SiO_4 amount. As shown in Fig. 5, M_2SiO_4 is consumed out at 1192 °C.

Based on Figs. 4–9, the formation of and change in the melts of CIC and OA–OD during heating are discussed as follows.

(1) Formation and change of CIC melt

At 1168–1175 °C: $(Fe, Al)_2O_3(s) + Ca(Fe, Al)_2O_4(s) + M_2SiO_4(s) \rightarrow Liquid(l) + Spinel(s) + O_2(g)$; at 1175 °C, $(Fe, Al)_2O_3$ is consumed out mainly owing to the decomposition to spinel.

At 1175–1178 °C: $Ca(Fe, Al)_2O_4(s) + M_2SiO_4(s) + Spinel(s) + O_2(g) \rightarrow Liquid(l)$; at 1178 °C, $Ca(Fe, Al)_2O_4$ is consumed out.

At 1178–1300 °C: M_2SiO_4 and spinel dissolve in the liquid, and M_2SiO_4 is consumed out at 1265 °C.

(2) Formation and change of OA–OD melts

At 1135–1136 °C: $Ca(Fe, Al)_2O_4(s) + Ca(Fe, Al)_6O_{10}(s) + M_2SiO_4(s) \rightarrow Liquid(l) + (Fe, Al)_2O_3(s) + O_2(g)$; at 1136 °C, $Ca(Fe, Al)_6O_{10}$ is consumed out.

At 1136 °C– T_c : $(Fe, Al)_2O_3(s) + Ca(Fe, Al)_2O_4(s) + M_2SiO_4(s) \rightarrow Liquid(l) + Spinel(s) + O_2(g)$. T_c is the characteristic temperature, at which $Ca(Fe, Al)_2O_4$ is consumed out. For OA–OD melts, T_c equals 1172, 1160, 1166, and 1159 °C, respectively.

At T_c –1183 °C: $(Fe, Al)_2O_3(s) + M_2SiO_4(s) \rightarrow Liquid(l) + Spinel(s) + O_2(g)$; at 1183 °C, $(Fe, Al)_2O_3$ is consumed out mainly owing to the decomposition to spinel.

At 1183–1300 °C: M_2SiO_4 and spinel dissolve in the liquid. For OA–OC melts, M_2SiO_4 is consumed out at 1192, 1258, and 1255 °C, respectively. OD melt will be described in the following.

$(Fe, Al)_2O_3$, calcium ferrites, M_2SiO_4 , and spinel take part in the formation of the liquid. The dissolution extent of calcium ferrites is larger than that of M_2SiO_4 . There are two kinds of calcium ferrites ($Ca(Fe, Al)_2O_4$ and $Ca(Fe, Al)_6O_{10}$) taking part in the formation of the liquid for OA–OD, whereas only $Ca(Fe, Al)_2O_4$ takes part in the formation for CIC. These indicate that calcium ferrites for CIC are more difficult than those for OA–OD to generate through solid-state reactions. The formation temperature of the liquid for CIC is 33 °C higher than that for OA–OD, that is to say, the liquid formation ability of CIC is weaker than that of OA–OD.

From Figs. 5–8, the formation temperatures of the liquid for OA–OD are the same. This can be explained as follows. According to Figs. 5–8 and the first period (1135–1136 °C) for the formation and change of OA–OD melts, calcium ferrites $Ca(Fe, Al)_2O_4$ and $Ca(Fe, Al)_6O_{10}$ are the main and fundamental substances for the formation of the liquid. As given in Table 2, for OA–OD adhering fines, abundant

Fe_2O_3 and CaO can be provided for the formation of calcium ferrites. In addition, in the equilibrium calculation of each adhering fines, there is enough time for the formation of calcium ferrites and further formation of the liquid. For iron ore fines OA–OD, the existing states of gangue components and LOI content may be different. During the actual sintering, the two factors may affect the reactivity of iron ore fines and dynamic conditions of solid-state reactions, and further the formation temperature of the liquid [11, 22]. It is a limitation of FactSage that the effects of the two factors on the formation of the melt cannot be calculated out. However, the calculation results of FactSage, especially the results regarding liquid amount and melt viscosity, can become references and basis for analyzing the formation and fluidity of the melt of iron ore fines.

It is worth noting that an auxiliary liquid exists in OD melt over the range of 1253–1269 °C. The amount of auxiliary liquid reaches its maximum value at 1256 °C, at which M_2SiO_4 is consumed out. Table 3 shows the chemical compositions, amounts, and viscosities of two liquids in OD melt at 1256 °C. The main components of the main liquid are Fe_2O_3 and CaO (their total content exceeds 83 mass%), and those of auxiliary liquid are Fe_2O_3 , CaO , and SiO_2 (their total content exceeds 91 mass%). They are non-miscible at certain temperatures [18]. The amount of the main liquid is higher than twice that of auxiliary liquid, whereas the viscosity of the main liquid is lower than half of that of auxiliary liquid.

From Fig. 8, when the temperature exceeds 1253 °C, auxiliary liquid starts to form through the reaction of the main liquid, spinel, and M_2SiO_4 . To clarify the reason why auxiliary liquid is formed, the chemical composition and viscosity of the liquid in OA–OD melts at 1253 °C (no auxiliary liquid) are given in Table 4. OD liquid has the highest Al_2O_3 content and viscosity at 1253 °C. High viscosity of OD liquid results from strong gravitation between molecules and ions [23], and thus, OD liquid has a very limited ability to further dissolve M_2SiO_4 and spinel. However, OD liquid can provide Al_2O_3 component for auxiliary liquid. M_2SiO_4 in OD melt has the highest amount among the four kinds of melts at 1253 °C and hence can provide CaO , SiO_2 , and small amounts of FeO and MgO for auxiliary liquid. Spinel can provide Fe_2O_3

and FeO components for auxiliary liquid. These components can react to form low-melting-point substances and melt into auxiliary liquid. Therefore, with abundant Fe_2O_3 and CaO for each kind of adhering fines, high contents of Al_2O_3 and SiO_2 are necessary conditions for the formation of auxiliary liquid. However, with further increasing the temperature, the viscosity of the main liquid decreases, and its dissolution ability is improved. When the temperature exceeds 1256 °C, auxiliary liquid starts to dissolve in the main liquid.

In order to investigate the equilibrium compositions of the melt, equilibrium tests were conducted on the five kinds of adhering fines referring to the experimental condition of MF test in Sect. 2.2. The soaking time of the adhering fines at 1300 °C in Fig. 2 extended from 4 min to 1 h to reach near-equilibrium states of the melts. After 1 h at 1300 °C, the melts were quenched by ice water (0 °C). The main mineral compositions of the melts after quenching were detected by XRD analysis. Figure 11 shows the XRD pattern of the melts after quenching. It can be seen that the main mineral in the melts after quenching is the solid solution of magnetite ($\text{Fe}_{2.950}\text{O}_4$ for CIC and $\text{Fe}_{2.932}\text{O}_4$ for OA–OD). Many weak miscellaneous peaks indicate that the crystallization of the liquid is extremely inferior. It is speculated that at 1300 °C, the melt contains liquid and the solid solution of magnetite. The experimental result basically agrees with the calculation result in Figs. 4–8.

As indicated in Fig. 11, a tiny amount of dicalcium silicate (Ca_2SiO_4) crystallizes from the liquid during quenching. A possible reason for this is that dicalcium silicate is more difficult than calcium ferrites to dissolve in the liquid during heating according to Figs. 4–8. Therefore, dicalcium silicate is easier than calcium ferrites to precipitate from the liquid during cooling.

3.2 MF of iron ore fines

Figure 12 shows ω of iron ore fines from the MF test in Sect. 2.2. ω of CIC is the lowest. For hematite ore, ω of OA is greatly higher than that of OB; for limonite ore, ω of OC is slightly higher than that of OD.

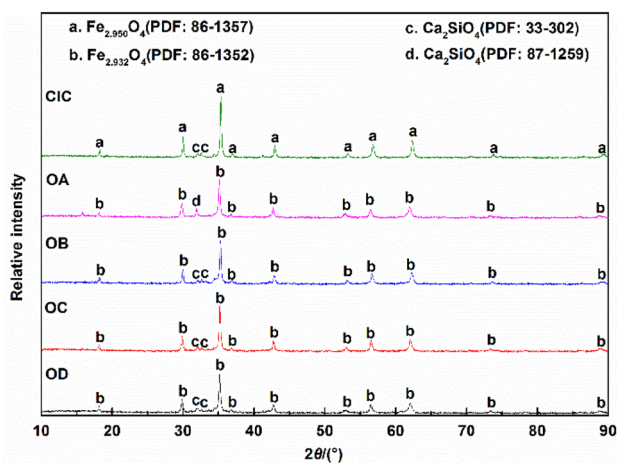
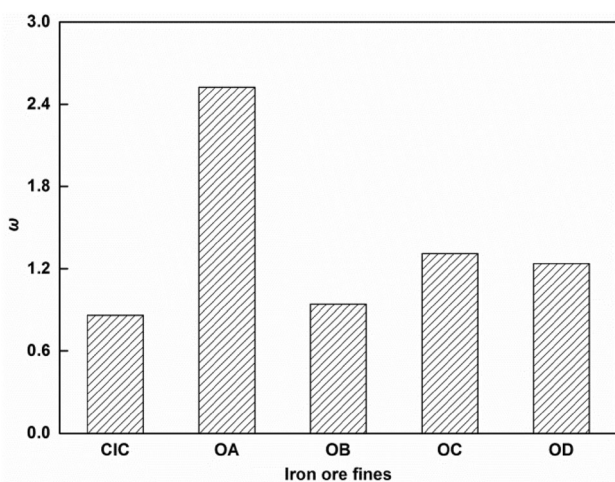
The chemical composition and proportion of the liquid in the melt at 1300 °C, from the theoretical calculation in

Table 3 Chemical compositions, amounts, and viscosities of two liquids in OD melt at 1256 °C in N_2 ($p_{\text{O}_2} = 101.325$ Pa)

Liquid	Chemical composition/mass%							Amount/g	Viscosity/ (Pa s)
	Fe_2O_3	FeO	SiO_2	CaO	Al_2O_3	MgO	Total		
Main liquid	62.84	8.76	5.44	20.81	2.13	0.02	100.00	45.54	0.042
Auxiliary liquid	47.80	7.02	14.26	29.30	1.59	0.03	100.00	19.01	0.092

Table 4 Chemical composition and viscosity of liquid in OA–OD melts at 1253 °C in N₂ ($p_{O_2} = 101.325$ Pa)

Liquid	Chemical composition/mass%							Viscosity/ (Pa s)
	Fe ₂ O ₃	FeO	SiO ₂	CaO	Al ₂ O ₃	MgO	Total	
OA	69.49	9.87	1.42	18.10	1.11	0.01	100.00	0.028
OB	63.91	8.77	4.91	20.40	2.00	0.01	100.00	0.040
OC	64.41	8.92	4.61	20.28	1.76	0.02	100.00	0.039
OD	64.59	8.49	4.42	19.93	2.55	0.02	100.00	0.041

**Fig. 11** XRD pattern of melts after quenching**Fig. 12** ω of iron ore fines

Sect. 3.1, are given in Table 5. According to the chemical composition of the liquid, the liquid viscosity was calculated through the Viscosity module of FactSage 7.2. The melt viscosity was calculated via Einstein–Roscoe model [24].

Figure 13 shows the relationships of ω of iron ore fines to calculated liquid amount and melt viscosity. Except for CIC, with increasing the liquid amount or decreasing the

melt viscosity, ω of iron ore fines increases. This is obvious and consistent with the results of previous researches [13, 18]. Moreover, the differences in the two calculated properties between hematite ores OA and OB are larger than those between limonite ores OC and OD. This leads to corresponding differences in ω in Fig. 12.

ω of CIC is below the curves, which may be related to the condition of the diffusion of Mg²⁺ into magnetite before the formation of the liquid. The experimental result of Panigrahy et al. [25] indicated that during heating, Mg²⁺ replaces some of Fe²⁺ from magnetite lattice by solid-state diffusion, forming mixed spinel ((Fe_{1-x}Mg_x)O·Fe₂O₃, $x \leq 1$). This is basically consistent with the calculation result given in Sect. 3.1. The Fe²⁺, released from the magnetite lattice, combines with O²⁻ and reacts with SiO₂ for initial slagging [25]. However, because the content of MgO in CIC is low, the amount of MgO around the magnetite is less. Thus, under the condition of rapid heating and short soaking time, the diffusion of Mg²⁺ into the magnetite lattice is weak, which depresses the initial slagging. Remaining Mg²⁺ may form more high-melting-point substances, such as Mg₂SiO₄ (melting point of 1890 °C). These decrease the liquid amount and increase the melt viscosity at same temperatures. Therefore, ω of CIC in the sintering test is lower than that under an equilibrium state.

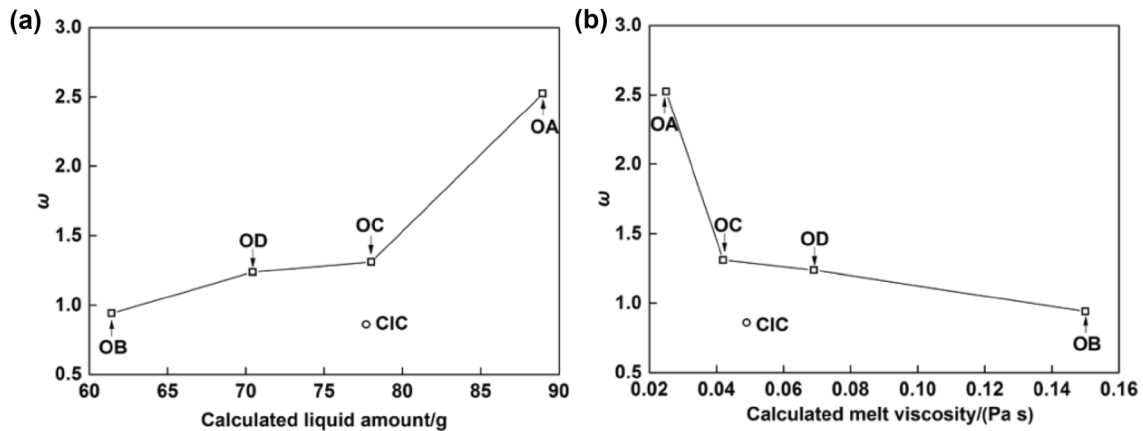
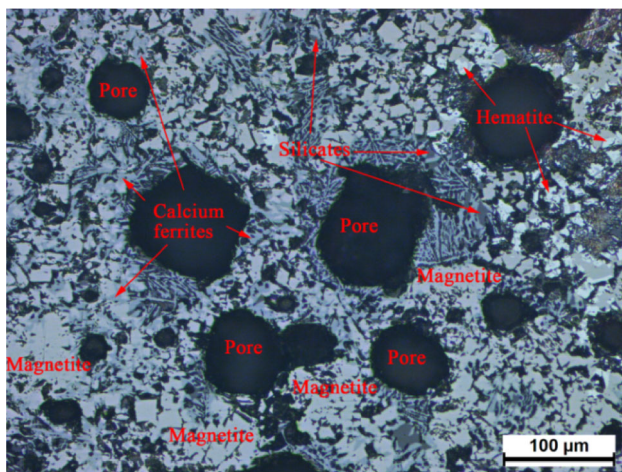
Figure 14 shows the microstructure mineralogy of CIC melt after cooling. As shown, the calcium ferrites are interweaved by the magnetite to form an interlaced corrosion structure; tiny amounts of the silicates distribute among the needlelike calcium ferrites; some residual hematite distribute around pores. It is speculated that under the condition of high-speed heating and short soaking time, much original or generated magnetite of CIC cannot dissolve in the liquid, which depresses the MF of CIC.

3.3 Penetration characteristic of CIC melt into iron ore nuclei

Figure 15 shows the microscopic morphology of the cross section of the sintered specimens and d of CIC melt into OA–OD nuclei. According to the distribution of pores and morphology of minerals, the penetration boundaries of CIC

Table 5 Calculated chemical composition and proportion of liquid, liquid viscosity, and melt viscosity at 1300 °C

Melt	Chemical composition of liquid/mass%							Proportion of Liquid/mass%	Viscosity/(Pa s)	
	Fe ₂ O ₃	FeO	SiO ₂	CaO	Al ₂ O ₃	MgO	Total		Liquid	Melt
CIC	62.68	12.19	4.76	19.99	0.18	0.20	100.00	79.73	0.028	0.049
OA	67.85	12.87	1.33	16.88	1.05	0.02	100.00	92.97	0.021	0.025
OB	53.37	10.24	10.83	24.47	1.07	0.02	100.00	63.86	0.049	0.150
OC	62.56	11.73	4.78	19.29	1.59	0.04	100.00	87.03	0.030	0.042
OD	58.40	11.00	7.37	21.37	1.83	0.04	100.00	78.90	0.038	0.069

**Fig. 13** Relationships of ω of iron ore fines to calculated liquid amount (a) and melt viscosity (b)**Fig. 14** Microstructure mineralogy of CIC melt after cooling

melt were determined and are shown as red curves in Fig. 15a. Obviously, the diameters of the sintered nuclei of limonite ores OC and OD are smaller than those of hematite ores OA and OB. This indicates that limonite ore nuclei have a significant contraction, which may be due to the release of too much crystal water from goethite at high temperatures. From Fig. 15b, the d values of CIC melt into hematite ore nuclei are larger than those of CIC melt into

limonite ore nuclei. A possible reason for this is that pores and cracks are formed after the dehydration of limonite ore nuclei, as shown in Fig. 15a. With the penetration of CIC melt into the nuclei, these pores and cracks enter into the melt and inhibit the further penetration of the melt [15]. Although d of CIC melt into limonite ore nuclei is smaller, much pores and cracks in the melt may be adverse to the strength of the sinter. For hematite ore nuclei, d for OB is larger than that for OA; for limonite ore, d for OC is slightly larger than that for OD. This means that much melt for OA and OD can be used to bond quasiparticles, which is conducive to the strength of the sinter [10].

A typical region of the cross section of the sintered specimens was analyzed through the scanning electron microscopy–energy dispersive spectroscopy (SEM–EDS) area mapping method. The cross section of the sintered specimens of CIC adhering fines and OA nuclei is shown as an example in Fig. 16. In Fig. 16, Fe uniformly distributes in the whole region, whereas Ca has a significant content gradient in the region. The distribution of Ca is consistent with the PD of CIC melt in Fig. 15a. It indicates that with the penetration of CIC melt into the nuclei, Ca in CIC melt diffuses into the nuclei and may combine with Fe, Si, or Al. A reaction zone between CIC melt and the nuclei is formed.

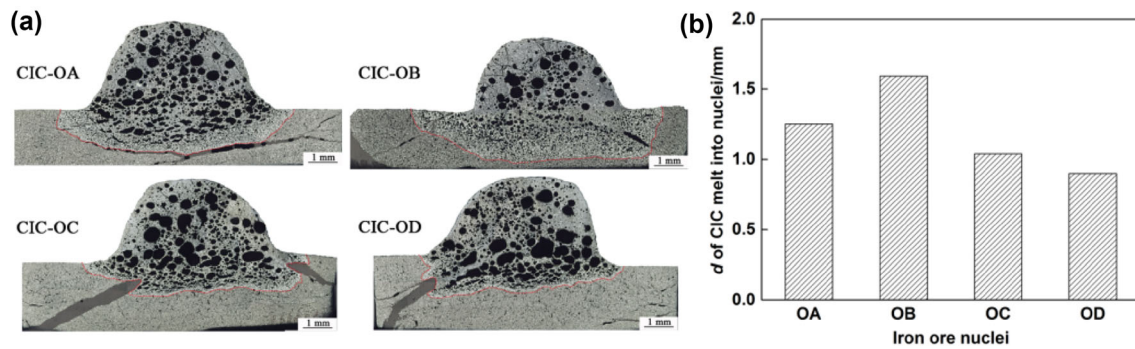


Fig. 15 Microscopic morphology of cross section of sintered specimens (a) and d of CIC melt into nuclei (b)

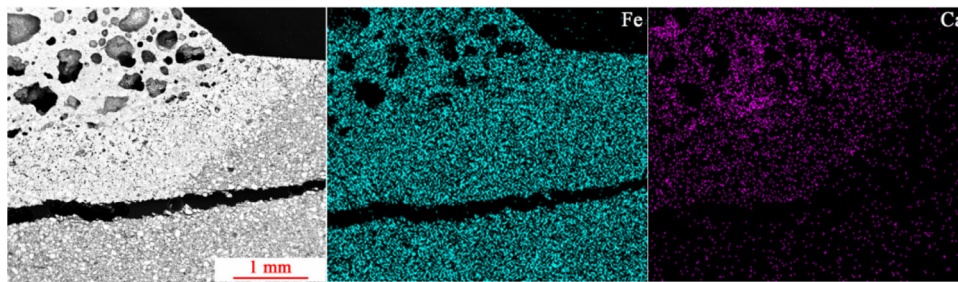


Fig. 16 Fe and Ca distribution maps of a typical region of cross section of sintered specimens of CIC adhering fines and OA nuclei

The same region of the cross section of the sintered specimens was analyzed via the SEM–EDS microanalysis method. The SEM micrographs and chemical compositions of points in reaction zone are presented in Fig. 17 and Table 6, respectively. In Fig. 17, the region is divided into three representative areas: CIC melt, reaction zone, and iron ore nuclei. The main minerals in the reaction zone are iron oxides (hematite or magnetite, white block in Fig. 17), silico-ferrites of calcium and aluminum (SFCA), and silicates. As given in Table 6, SFCA are the calcium ferrite phases containing some silica and alumina, and silicates are the calcium silicate phases dissolving some alumina and iron oxides [26]. There exists a tiny amount of Mg element in the SFCA and silicates. The SFCA and silicates precipitate from the secondary melt, which is formed by the reaction of CIC melt and the nuclei [10].

For hematite ore nuclei, the contents of Al and Si in the SFCA for OA are higher than those for OB, and the contents of Al and Fe in the silicates for OA are higher than those for OB. This indirectly indicates that the secondary melt formed by CIC melt and OA nuclei dissolves more acid components than that formed by CIC melt and OB nuclei. OA nuclei have stronger reaction ability than OB nuclei with CIC melt. These acid components increase the viscosity of the secondary melt, inhibiting the penetration of the melt into the nuclei [10].

Thus, d of CIC melt into OA nuclei is smaller than that of CIC melt into OB nuclei.

For limonite ore nuclei, the contents of Al and Si in the SFCA for OC are higher than those for OD, and the contents of Al and Fe in the silicates for OC are higher than those for OD. This implies that OC nuclei have stronger reaction ability than OD nuclei with CIC melt. Different from hematite ore nuclei, limonite ore nuclei have less acid components and more space at a same site owing to the release of massive crystal water. As a result, the stronger the reaction ability of the nuclei with CIC melt, the larger d of CIC melt into the nuclei. Thus, d of CIC melt into OC nuclei is larger than that of CIC melt into OD nuclei.

The research result of Okazaki et al. [15] showed that using a mixture of Fe_2O_3 and CaO (1:1 in mol) as the adhering fines, the d values of calcium ferrite melt into hematite and limonite ore nuclei at 1290 °C in air are over the range of roughly 3.8–4.2 mm and 1.2–1.4 mm, respectively. Those values are larger than those shown in Fig. 15b. Through the calculation of FactSage 7.2, it is found that the viscosity of calcium ferrite melt at 1290 °C in air is 0.034 Pa s, which is lower than that of CIC melt (0.049 Pa s) at 1300 °C in N_2 ($p_{\text{O}_2} = 101.325$ Pa). Hence, d in previous study [15] is larger than that in this study.

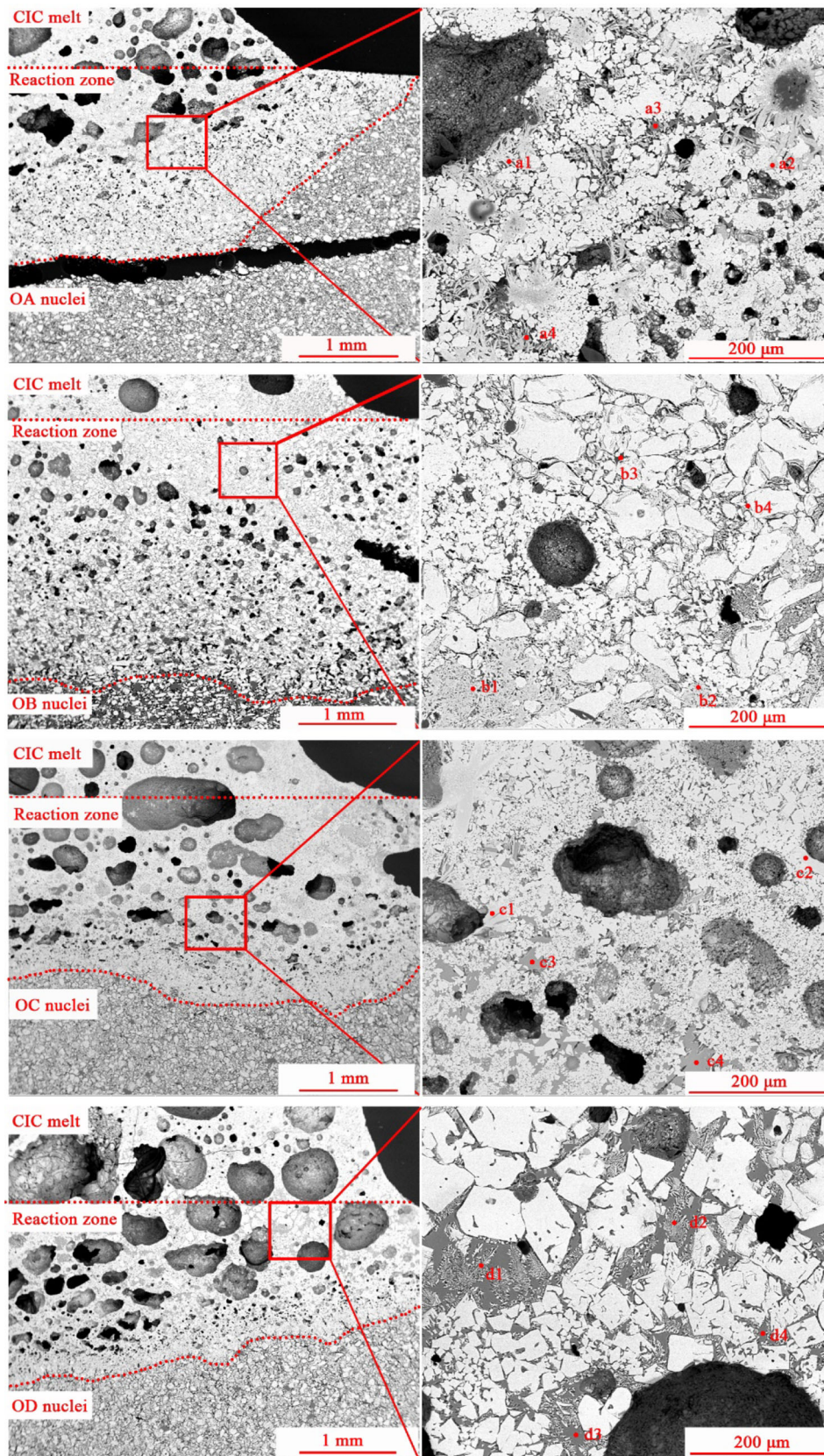


Fig. 17 Micrographs of typical region of cross section of sintered specimens obtained by SEM

Table 6 Chemical compositions of points in reaction zone of sintered specimens obtained by EDS (mass%)

Point	Mineral	O	Mg	Al	Si	Ca	Fe	Total
a1	SFCA	23.41	0.31	1.54	4.58	11.37	58.79	100.00
a2	SFCA	25.78	0.47	3.82	5.74	12.32	51.87	100.00
a3	Silicates	28.51	0.15	3.06	22.11	32.44	13.73	100.00
a4	Silicates	28.87	0.23	2.06	22.32	33.08	13.44	100.00
b1	SFCA	22.69	0.30	0.52	4.46	15.91	56.12	100.00
b2	SFCA	18.96	0.58	0.32	2.70	10.34	67.10	100.00
b3	Silicates	34.99	0.28	0.19	12.87	46.86	4.81	100.00
b4	Silicates	33.08	0.22	0.00	14.06	45.08	7.56	100.00
c1	SFCA	21.93	0.56	2.56	3.74	10.34	60.87	100.00
c2	SFCA	23.07	0.84	1.97	3.51	10.67	59.94	100.00
c3	Silicates	27.53	0.58	3.72	20.95	32.04	15.18	100.00
c4	Silicates	28.94	0.79	3.52	20.30	30.69	15.76	100.00
d1	SFCA	23.37	0.32	0.64	1.52	9.51	64.64	100.00
d2	SFCA	23.86	0.00	0.32	2.76	9.14	63.92	100.00
d3	Silicates	27.05	0.55	2.50	22.84	33.38	13.68	100.00
d4	Silicates	27.42	0.38	1.42	22.57	33.67	14.54	100.00

4 Ore-blending optimization study

From the MF of iron ore fines, the MF of hematite ore OA is considerably higher than that of OB, and the MF of limonite ore OC is slightly higher than that of OD. From the penetration characteristic of CIC melt into iron ore nuclei, the PD for hematite ore OA is significantly smaller than that for OB, and the PD for limonite ore OC is slightly larger than that for OD. The differences between OC and OD in the MF and penetration characteristic are insignificant and contradictory; thus, the ore-blending optimization based on the substitution between OC and OD is expected to be inefficient. Therefore, under unchanging the usage ratio of hematite ore to limonite ore (limited by resources condition), replacing OB with OA in ore blends may significantly improve the MF of adhering fines and weaken the penetration characteristic of the melt into iron ore nuclei. Furthermore, this can improve the bonding strength of the sinter [10, 13, 22].

To investigate the effect of CIC on sintering indexes and the feasibility of above method, some schemes of sinter pot tests were conducted. The ore-blending structures of the ore blends are given in Table 7. In these ore blends, the proportions of undersieves and accessory materials were fixed. When the proportion of CIC increased (0 → 10 → 15 mass%), the proportions of OA–OD decreased correspondingly according to their ratio in base scheme. Optimization-1 and optimization-2 were optimization schemes via replacing half of OB with OA based on schemes CIC-10 and CIC-15, respectively. The

proportions of quicklime, return fines, and fuel in the blending material were 4.00, 25.00, and 4.00 mass%, respectively. SiO₂ content, MgO content, and binary basicity of the sinter were set as 5.00 mass%, 1.45 mass%, and 1.80, respectively, through adjusting the proportions of limestone, dolomite, and serpentine. Approximately 42 kg of blending material was mixed uniformly and then granulated for 3 min in a drum granulator with a diameter of 650 mm and a height of 600 mm under a moisture of 8 mass%. The granulated blending material is then sintered in a sinter pot with an inner diameter of 230 mm and a height of 680 mm under a suction of 10 kPa.

The sintering indexes of sinter pot test are given in Table 8. The chemical composition and proportion of the adhering fines in the blending material are presented in Table 9 to analyze the effect of CIC on the adhering fines. From Table 8, with increasing the proportion of CIC, the vertical sintering speed, yield, productivity, and tumbler index (TI) decrease. A possible reason for the decrease in the vertical sintering speed is that almost all the CIC enters into the adhering fines, and the proportion of the adhering fines increases from 27.49 to 33.43 mass%. This may influence the granulation effectiveness of the quasiparticles and hence the permeability of the sintering bed [16]. In addition, with a similar SiO₂ content to that of the adhering fines in base scheme, CIC dilutes the CaO content and hence decreases the binary basicity of the adhering fines. The reduction in the binary basicity and low MF of CIC depress the MF of the whole adhering fines, which is adverse to the bonding of the quasiparticles and the strength of the sinter [14, 22]. Therefore, the yield and TI

Table 7 Ore-blending structure of ore blends (mass%)

Scheme	CIC	OA	OB	OC	OD	Undersieves	Accessory material	Total
Base	0.00	18.00	16.00	38.00	13.00	10.00	5.00	100.00
CIC-10	10.00	15.88	14.12	33.53	11.47	10.00	5.00	100.00
CIC-15	15.00	14.82	13.18	31.29	10.71	10.00	5.00	100.00
Optimization-1	10.00	22.94	7.06	33.53	11.47	10.00	5.00	100.00
Optimization-2	15.00	21.41	6.59	31.29	10.71	10.00	5.00	100.00

Table 8 Sintering indexes of sinter pot test

Scheme	Vertical sintering speed/ (mm min ⁻¹)	Yield _{+5 mm} /mass%	Productivity/ (t m ⁻² h ⁻¹)	TI _{+6.3 mm} /mass%
Base	29.04	79.95	2.16	63.33
CIC-10	25.42	78.19	1.87	62.67
CIC-15	24.12	77.41	1.67	62.43
Optimization-1	28.57	79.81	2.18	64.00
Optimization-2	27.15	78.36	2.04	63.00

Table 9 Chemical composition and proportion of adhering fines in blending material (mass%)

Scheme	TFe	SiO ₂	CaO	Al ₂ O ₃	MgO	R	Proportion
Base	48.18	4.41	15.25	1.17	1.43	3.45	27.49
CIC-10	50.54	4.40	13.46	0.99	1.33	3.06	31.45
CIC-15	51.51	4.40	12.72	0.92	1.28	2.89	33.43
Optimization-1	50.01	4.28	14.21	1.00	1.38	3.32	29.90
Optimization-2	51.09	4.30	13.35	0.92	1.33	3.11	31.98

of the sinter are reduced. The productivity of the sinter decreases owing to the comprehensive effect of the vertical sintering speed and yield. The benefit of adding CIC in ore blends is reflected in elevating the ferrous grade and reducing the contents of Al₂O₃ and MgO, as given in Table 9.

Comparing the sintering indexes of schemes CIC-10 and CIC-15, those of schemes optimization-1 and optimization-2 are significantly improved, respectively. The sintering indexes of optimization-1 are very close to those of base scheme. Without deteriorating the sintering indexes significantly, 10 mass% is suggested as a suitable proportion for adding CIC in the present ore blends. According to previous researches [4, 5], when replacing OB with OA, the growth index of the quasiparticles and vertical sintering speed increase owing to the improvement in granulation behavior of fines and nuclei of iron ore. On the other hand, after replacing OB with OA, the proportion of the adhering fines decreases, and the binary basicity of the adhering

fines increases. Moreover, the MF of iron ore fines and penetration characteristic of the melt into iron ore nuclei are improved. These are conducive to the sintering indexes according to previous analysis in this study.

5 Conclusions

1. Hematite, calcium ferrites, dicalcium silicate, and magnetite take part in the formation of the liquid in N₂. The dissolution extent of calcium ferrites is larger than that of dicalcium silicate. The formation temperature of the liquid for CIC is higher than that for hematite/limonite ore fines.
2. An auxiliary liquid for iron ore fines with high contents of Al₂O₃ and SiO₂ exists over a certain temperature range. The amount of the main liquid is greatly higher than that of auxiliary liquid, whereas the viscosity is the opposite.

3. The liquid amount and melt viscosity have positive and negative effects on the MF of hematite/limonite ore fines, respectively. The MF of CIC is lower than that of hematite/limonite ore fines.
4. The PD of CIC melt into limonite ore nuclei is smaller than that into hematite ore nuclei. For hematite ore, the PD of CIC melt into strong-reaction-ability nuclei is smaller than that into weak-reaction-ability nuclei, whereas the PD of CIC melt for limonite ore is the opposite.
5. CIC deteriorates the sintering indexes. Increasing the proportion of high-MF and small-PD hematite ore can significantly improve the sintering indexes. 10 mass% is a suitable proportion for adding CIC in ore blends.

Acknowledgements The authors are grateful for the financial support of the Fundamental Research Funds for the Central Universities (Grant No. FRF-IC-18-010).

References

- [1] D.Q. Zhu, H. Wang, J. Pan, C.C. Yang, J. Iron Steel Res. Int. 23 (2016) 661–668.
- [2] G. An, Z.X. Zhao, M. Xu, X.D. Zhang, J.L. Zhang, Iron and Steel 43 (2008) No. 9, 8–11.
- [3] M. Gan, X.H. Fan, Z.Y. Ji, X.L. Chen, L. Yin, T. Jiang, Z.Y. Yu, Y.S. Huang, Ironmak. Steelmak. 42 (2015) 351–357.
- [4] Z.G. Que, S.L. Wu, X.B. Zhai, K.L. Li, Ironmak. Steelmak. 46 (2019) 246–252.
- [5] S.L. Wu, Z.G. Que, X.B. Zhai, K.L. Li, Metall. Res. Technol. 115 (2018) 202.
- [6] D.Q. Zhu, Y. Zhong, J. Pan, Chin. J. Eng. 37 (2015) 984–993.
- [7] J. Pan, D.Q. Zhu, P. Hamilton, X.L. Zhou, L. Wang, ISIJ Int. 53 (2013) 2013–2017.
- [8] J. Pan, B.J. Shi, D.Q. Zhu, Y.P. Mo, ISIJ Int. 56 (2016) 777–785.
- [9] F. Zhang, D.Q. Zhu, J. Pan, Y.P. Mo, Z.Q. Guo, Int. J. Miner. Metall. Mater. 25 (2018) 598–608.
- [10] S.L. Wu, B. Su, Y.H. Qi, M.Y. Kou, Y. Li, W.L. Zhang, Metall. Mater. Trans. B 48 (2017) 2469–2480.
- [11] G.L. Zhang, S.L. Wu, S.G. Chen, B. Su, Z.G. Que, C.G. Hou, Int. J. Miner. Metall. Mater. 21 (2014) 962–968.
- [12] D.M. Liu, C.E. Loo, G. Evans, Int. J. Miner. Process. 149 (2016) 56–68.
- [13] J. Peng, L. Zhang, L.X. Liu, S.L. An, Metall. Mater. Trans. B 48 (2017) 538–544.
- [14] S.L. Wu, B. Su, Y.H. Qi, Y. Li, B.B. Du, Chin. J. Eng. 40 (2018) 321–329.
- [15] J. Okazaki, K. Higuchi, Y. Hosotani, K. Shinagawa, ISIJ Int. 43 (2003) 1384–1392.
- [16] Z.X. Xiao, Z.L. Xue, Z.G. Hu, Z.J. Wen, Research on Iron Steel 41 (2013) No. 6, 1–6.
- [17] L.X. Yang, ISIJ Int. 45 (2005) 469–476.
- [18] X.B. Zhai, S.L. Wu, H. Zhou, L.X. Su, X.D. Ma, Ironmak. Steelmak. (2019-05-21): <https://doi.org/10.1080/03019233.2018.1537223>.
- [19] Y.J. Liang, Y.C. Che, The handbook of inorganic thermodynamics data, Northeastern University Press, Shenyang, China, 1993.
- [20] CRCT, FactSage 7.2, 2006 (2019-05-21). <http://www.factsage.cn/>.
- [21] J.W. Jeon, S.M. Jung, Y. Sasaki, ISIJ Int. 50 (2010) 1064–1070.
- [22] S.L. Wu, G.L. Zhang, S.G. Chen, B. Su, ISIJ Int. 54 (2014) 582–588.
- [23] K. Wu, Metallurgical transmission principle, Metallurgical Industry Press, Beijing, China, 2011.
- [24] Z.Q. An, Y.L. Zhang, Q. Li, Z.C. Guo, Mater. Sci. Eng. Powder. Metall. 20 (2015) No. 1, 46–52.
- [25] S.C. Panigrahy, P. Verstraeten, J. Dilewijns, Metall. Trans. B 15 (1984) 23–32.
- [26] N.A.S. Webster, M.I. Pownceby, I.C. Madsen, J.A. Kimpton, Metall. Mater. Trans. B 43 (2012) 1344–1357.